Robot-assisted superficial hyperthermia treatments: the ROBHOT system

Marco Ferro[1,*], Pierfrancesco Pavoni[2], Marilena Vendittelli[1]

***Abstract*— This paper presents the design, implemetation and experimental validation of the ROBHOT Technology Demonstrator, a new system for robot-assisted superficial hyperthermia treatments. The system features impedance-based interaction control for accurate and safe delivery of the treatment, a digital twin of the operative setup, communication modules with a pre-operative planning software. Results of the system validation in a relevant experimental environment are reported. A video clip presenting an overview of the system and the validation experiments is available at `https://youtu.be/rNxMaD-teNo`.**

I. INTRODUCTION

In oncology, hyperthermia (HT) is a treatment used to increase the efficacy of chemotherapy (CT) and radiotherapy (RT) in terms of complete response, local tumour control and overall survival [1]. HT aims at rising the temperature in tumorous tissues to the range of 40-45°C for about 60 min to induce: (i) inhibition of tumour cell repair mechanisms to recover from the damage caused by radiotherapy; (ii) increase of blood flow and, hence, re-oxygenation with a consequent powerful radio-sensitizing effect, and greater transport of the chemo agent to the tumour site; (iii) increase of the cell membrane permeability allowing an increase in the uptake of chemotherapeutic agents. Tissue temperature raising is due to absorption of an electromagnetic field at radio/microwave frequencies radiated by one or more antennas. Superficial HT, in particular, is used to treat tumours located at depths of 4/5 cm maximum under the patient's skin and the radiating antenna is placed on the body surface at the tumour site. Despite solid scientific foundation and clinical evidence [2]–[6], current procedures do not meet the level of accuracy, integration in the RT workflow, and procedural timing required to guarantee full exploitation of the treatment potential [7]–[9]. As a matter of fact, clinical outcomes of the combined HT-CT and/or HT-RT treatments are critically related to the ability of reaching and maintaining temperatures at the desired target, with the right timing, for the desired duration, in a reproducible manner for all the subsequent HT treatments [10]–[14]. These quality requirements are hard to achieve in tumours typically treated with superficial HT like, e.g., breast, head and neck, and skin/extremities cancers, because of their significant differences in both size and morphology, and for the anatomical complexity in their location which complicates the antenna placement. Currently, RF antennas for superficial HT are positioned manually to a location indicated by the clinician, through a passive mechanical arm, without any sort of feedback information on the antenna positioning. Once settled in position, the arm is fixed to try to hold the location for the whole 60 minutes duration of the treatment. Clearly, this manual process hinders the possibility of reproducing the same position of the microwave applicator in the subsequent HT sessions, over the several weeks of the therapy; it does not allow for an automatic tracking of the microwave applicator pose in case of patient's movements during each of the 60-min treatment, thus moving the electromagnetic field focus and, hence, possibly degrading the quality of the HT treatment and/or causing the irradiation of healthy, delicate or at risk organs; it presents longer procedural time and lower accuracy with respect to the standards of RT.

The recently proposed ROBHOT[1] system aims at removing these obstacles through the introduction of robots and robotic technologies in the HT treatment. ROBHOT features a PANDA manipulator to safely move the antenna mounted at its end-effector for placing and keeping it in contact with the patient for the whole treatment (see Fig. 1), despite patient's volutary or involutary motion. The Polaris optical localization and tracking system provides information for registration of the pre-operative radiation plan. Data from the robot and the optical sensor are sent to a digital twin that includes also a 3D model of the patient to be treated.

To our best knowledge, this is the first example of a superficial HT system supported by robot that can guarantee accurate registration of the pre-operative plan, safe and comfortable antenna positioning, from the preparation phase to the delivery of the treatment. Related systems include [15] which, however, uses hyghly focused ultrasoud, a different technology with similar terapeutic objective. It does not include a digital twin and the interaction force is monitored to be below a prescribed threshold but not controlled so as to guarantee a compliant behaviour of the robot, according to a properly designed model of the interaction.

From the robotic point of view, the problems to be solved are related to the registration of the pre-operative

*corresponding author

[1]The authors are with Department of Department of Computer, Control, and Management Engineering "Antonio Ruberti", Sapienza University of Rome, Via Ariosto 25, 00185, Rome, Italy. {ferro, vendittelli}@diag.uniroma1.it

[2] Medlogix Srl, Via Adriano Olivetti, 24, 00131 Rome, Italy, pf.pavoni@medlogix.eu

This work has been partially supported by the DIH HERO and the Sapienza Project RM120172AD69A503 "Development of innovative superficial hyperthermia applicators including automatic real-time adjustments for treatment optimization".

[1]ROBHOT is a Technical Demonstrator developed by the authors with the financial support of the Digital Innovayion Hub HERO.

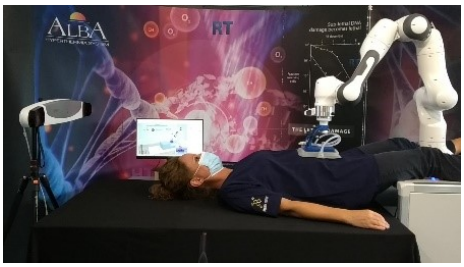

Fig. 1: The ROBHOT system: the superficial HT antenna is safely and accurately placed and kept in contact with the patient body, at the desired pose, by a FRANKA EMIKA PANDA manipulator integrating the information from the Polaris optical localization and tracking system and of a digital twin of the whole operating scenario.

plan in the reference frame of the robot and the control of the physical human-robot interaction occurring both in the manual guidance of the robot (positioning of the robot in the initial phase of the procedure by a human operator) and during the delivery of the treatment, when the antenna must be kept in contact with the patient.

For the localization and tracking problem we use a deterministic Iterative Closest Point algorithm [16]. The state of the art on robot interaction control includes well known and established direct and indirect force control schemes: impedance/admittance control, force control, hybrid force/position control and compliance control [17]. Each of them are largely employed in the different fields of robotics for specific applications. In the medical robotics field, the control objective is to determine autonomous or semi-autonomous behaviours based on safe interaction also with delicate anatomical structures, that could minimize stress and pain for the patient. For these reasons, different control solutions are proposed [18]. In [19], a control architecture for compliant comanipulation, for robot-assisted medical procedures, is presented. The described method implements an impedance control, both passive and active, on the position of the employed medical device, in order to establish the desired dynamic interaction between the robot and a human cooperator. In [20], the authors present a method for the control of a ultrasound (US) probe, manipulated by a robotic system. The presented strategy regulates the interaction force of the probe with the target surface, while simultaneously accomplishing additional visual control objectives based on the acquired images. Other examples of interaction control approaches, based on impedance control schemes, have been employed for beating-heart surgery [21]. More recently, a very close system architecture and interaction control has been proposed in [22] for robot-assisted ultrasound tissue scanning.

In this work, we present design and validation results of the ROBHOT Technology Demonstrator, a new treatment system integrating a complete software framework allowing seamless transfer from simulation to experiments. In the real operative scenario, this means that it will allow to move from planning to treatment delivery in a seamless and fast way. The system includes a digital twin of the operating system, communication modules with a pre-operative planning software, the possibility to integrate different devices to interact with the system, the possibility to easily extend the framework to different technology-assisted medical procedures.

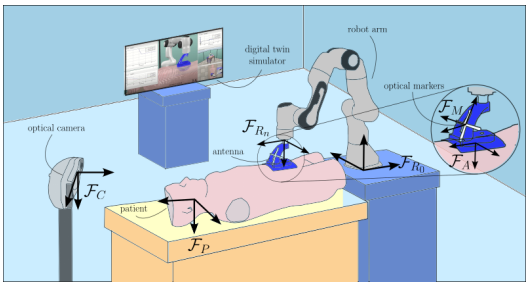

Fig. 2: Representation of the experimental setup.

ROBHOT is characterized by a continuous physical interaction between the patient and the involved medical devices mounted at the robot end-effector. The proposed control approach provides an easy manual guidance of the robot for gross positioning and fast removal from the operating field and a desired compliant interaction behavior of the robot to accomodate physiological and unadverted movements of the patient during the treatment, in order to guarantee safety in the executed procedures. The controllers are validated on the real system, in an operational environment.

II. ROBHOT System Architecture

Robot assistance and full automation of superficial HT will allow reaching the accuracy level of radiotherapy in treatment delivery and will increase patient safety and comfort. The ROBHOT technical demonstrator presented in this paper is the cornerstone of the whole project providing: i) accurate antenna positioning with respect to the anatomical target of interest; ii) visual monitoring of the procedure progress through a *digital twin* of the ROBHOT system including a 3D model of the patient; iii) guarantee of comfort and safety of the patient throughout the treatment.

To achieve these objectives the technological setup includes: i) an NDI Polaris Vega optical camera with optical markers, to enable real-time tracking of the antenna; ii) a Franka Emika Panda robot, for shared and autonomous positioning of the antenna on the identified target; iii) an external CoppeliaSim simulation software for 3D rendering and simulation of the scenario core components; iv) a dedicated software with layered architecture and modules enabling communication and interaction between the components listed above and designed to allow integration of additional components. Fig. 2 reports the involved components and highlights the relevant reference frames involved in the system: $\mathcal{F}_C$ is the reference frame attached to the optical camera; $\mathcal{F}_{R_0}$ and $\mathcal{F}_{R_n}$ are the reference frame attached to the base and the tip of the robot, respectively; $\mathcal{F}_A$ is the reference frame attached to the radiative antenna mounted at the end-effector of the robot; $\mathcal{F}_M$ is the reference frame attached to the optical markers mounted on the antenna, to allow real-time tracking through the camera; $\mathcal{F}_P$ is the reference frame attached to the patient/target anatomy of interest.

The remainder of this Section provides technical details about these components.

A. NDI Polaris Vega ST optical camera

The NDI Polaris Vega ST[2] in Fig. 3 is an optical system largely used in clinical environments to track the pose of objects and instruments in real-time, based on near-infrared (IR) light technology. The system toolkit is composed of: i) a dedicated camera (Figure 3a), retrieving optical measurements with sub-millimeter accuracy (0.12mm) at rates of 20, 30 or 60 Hz within a pyramid measurement volume, with an average latency < 16ms; a set of 4 passive optical markers mounted on a rigid-body frame (Figure 3b), to be attached on the clinical instrument to track; iii) a probe equipped with 4 passive optical markers (Figure 3c), used for intra-operative patient registration, and hence for subsequent transfer of a pre-operative plan to the robot; iv) a set of API functions required to query the system and to develop custom applications.

In the ROBHOT system, a 4-marker rigid-body frame is mounted on the holder of the radiative antenna, as shown in Fig. 3d, for tracking pourposes. The passive probe is used for patient-Polaris intra-operative registration, as will be detailed in Sect. III-A. Finally, the API functions have been integrated in a dedicated *proxy* class of the ROBHOT control software architecture, as detailed in Sect. II-D.

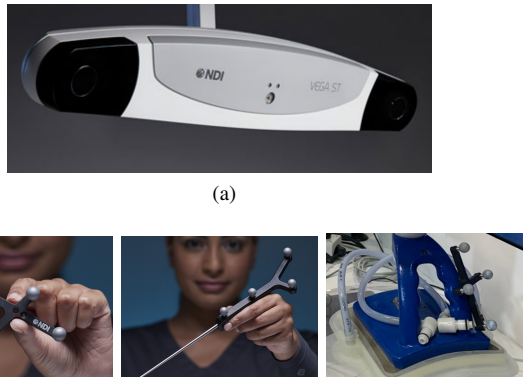

(a)

(b) (c) (d)

Fig. 3: The NDI Polaris Vega system: (a) the optical camera; (b) the rigid-body frame hosting a set of 4 optical markers, here attached to the radiative antenna for tracking; (c) the optical passive probe, here used to implement the registration routine of the Polaris system with respect to the environment; (d) the NDI rigid-body frame attached to the radiative antenna in the ROBHOT system.

B. Franka Emika PANDA robot manipulator

The Franka Emika PANDA[3] (featured in Figure 1) is a fixed-based robot manipulator arm with 7 degrees of freedom, equipped with encoders and link-side torque sensors at each joint. The platform weight is around 18Kg, with the possibility to hold payloads at the end-effector up to 3Kg, which is sufficient to hold standard radiative antennas and the *water bolus* required to cool the skin during superficial hyperthermia treatments. The robot guarantees a positioning accuracy during motion of $<$ 1.25mm, while the force (torque) sensing resolution is $<$ 0.05N ($<$ 0.02Nm). A Franka Control Interface (FCI) enables, at the robot-side, the low-level control of the platform at 1KHz, while the dedicated open-source C++ library `libfranka` runs at client-side to manage the UDP-based network communication and to provide the functionalities for reading the robot state and send input commands from an external application. Input commands can be position or velocity in the Cartesian or in the joint space, executed by the low-level motion generator module of the FCI. Alternatively, direct control of joint motors is also possible by sending appropriate joint torque commands. These functionalities and the access to the `libfranka` library have been integrated in a dedicated *proxy* class of the ROBHOT software solution, as detailed in Sect. II-D.

[2]`https://www.ndigital.com/`
[3]`https://www.franka.de/`

C. CoppeliaSim simulation software

CoppeliaSim (formerly V-REP) is a simulation software that offers a dedicated and versatile development environment for robot motion planning and control, by providing tools to program multi-robot applications in different programming languages (C/C++, Python, Java, Lua, Matlab, Octave) and implementation solutions (embedded plugin, ROS note, external remote API client). The high degree of customization of the virtual scene makes the simulator ideal for building the *digital twin* of our system, i.e., a virtual reconstruction of the operative environment with enhanced visualization and signal monitoring properties. In ther ROBHOT system, the CoppeliaSim remote API functions have been chosed to interconnect the simulator with the the robot and the optical camera, wrapped in a dedicated *proxy* class of the proposed software architecture, as detailed in Sect. II-D.

D. Software architecture

The multi-layer ROBHOT software architecture is depicted in Fig. 4a, as a slight modification of the framework that we have also presented in [23].

The top layer (highlighted in blue in in Fig. 4a) is responsible of interfacing the external systems involved in the environment with the functionalities of the software implemented at the lower levels. This is achieved through a set of *proxy* objects that exchange data with each system trough dedicated libraries and SDKs. Currently they include the Franka robot, the Polaris optical camera, the CoppeliaSim simulator, and a user interface required to provide inputs about procedures to run. This last functionality is not used in ROBHOT but it is useful to validate the interaction control strategies in simulation. It also enlighten the flexibility of the framework in allowing seamless extension to remotely operated procedures.

At the middle layer (yellow box in Fig. 4a), we consider objects implementing high-level routines that need to gather and coordinate data from different proxies of the higher level, to update the state of the environment stored in the lower levels. This involves task- and control-related procedures (e.g., registration, antenna tracking and robot-assisted placement). Furthermore, at this level we implement the different robot control strategies that will be compared to assess the effectiveness with respect to the treatment requirements.

The objects at the lower layer (red in Fig. 4a) refer to atomic components of the setup (e.g., robot, antenna, target volume) or mathematical tools (e.g., algorithms, filters), describing the current state of the environment. These objects are used by the higher-level routines to run storing/loading operations and processing of local data (e.g., update of the robot state, execution of the ICP algorithm for registration). Actual write-read operations on the file-system of each component are finally achieved in the last layer of the architecture (gray box in Fig. 4a).

Proxies, task and controller objects of the higher layers execute their own routines through dedicated threads. On one side, proxies threads periodically refresh data exchanged with the external systems and share them with the task-level routines. On the other side, task and controller threads collect such data from the proxies, execute their own routine and mutually get access to the state of the environment at the lower level (see Fig.4b). Video clip of the ROBHOT Digital Twin.

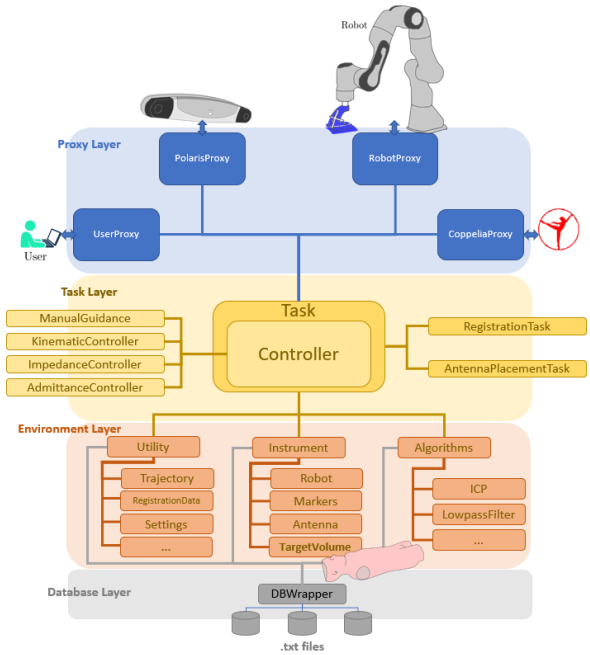

(a)

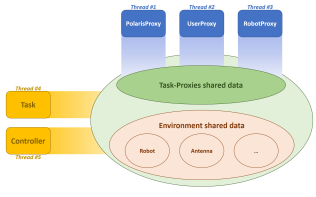

(b)

Fig. 4: The ROBHOT software architecture: (a) Flowchart of the implemented multi-layer architecture, managing the communication with the involved external systems, the execution of the treatment routines, the control of the robot and the update of th environment state. (b) Scheme of the multi-threading communication among the different components of the architecture.

III. HYPERTHERMIA TREATMENT AUTOMATION

The integration of the NDI Polaris optical camera and the Franka Emika Panda manipulator into the clinical setting allow to perform the treatment procedure with *assisted* manual antenna positioning, facilitated by real-time tracking of the antenna using the optical camera. Additionally, it offers the option for *autonomous* or *semi-autonomous* antenna positioning, leveraging the high accuracy and repeatability of the robot to control the antenna's pose and respond actively to unintended physiological motions of the patient, such as breathing.

In both considered treatment modalities, the setup integrates a a virtual replica of the clinical scenario (*digital twin*) implemented in the CoppeliaSim environment. This includes a 3D model of the anatomical region of interest, reconstructed from available preliminarily acquired CT scans. The scans are available from the pre-operative phase of the treatment, as they are used by the clinicians to plan the desired location of the antenna, so as to have the target tumor within the maximum Specific Absorption Rate (SAR) volume of the antenna.

The pre-operative planning phase of the hyperthermia treatment provides the desired pose for the antenna with respect to the patient reference frame. However, in order to quantitatively assess the accuracy of the positioning procedures, it is necessary to transfer the treatment plan from the target anatomy to the robot and camera reference frames. For this purpose, we implemented a registration procedure based on *fiducial* marker, in order to estimate the camera-patient and robot-patient spatial relationships. In the remainder of this Section, we will detail first the registration procedure for the camera and the robot systems. Then, we will describe the optical-based and robot-based treatment modalities offered by the ROBHOT system.

A. Registration

With reference to the frames already specified in Fig. 2 and listed in the previous Section, the marker-based registration procedure estimates the 4×4 homogeneous transformation matrices ${}^{P}\boldsymbol{T}_{C}$ and ${}^{P}\boldsymbol{T}_{R}$, denoting the relative pose of the robot and camera frames $\mathcal{F}_{R_0}$ and $\mathcal{F}_{C}$ with respect to the patient frame $\mathcal{F}_{P}$, respectively.

In detail, 4 radiopaque markers are preliminarily applied on the target anatomy, to allow visualization in the CT scans and retrieve direct measurements of the corresponding coordinates ${}^{P}\boldsymbol{p}_{i} \in \mathcal{F}_{P}$, for $i = 1, \ldots, 4$. In order to correctly achieve the designed marker-based registration, it is necessary to acquire the coordinates of the same points in the target reference frame to be registered, i.e., ${}^{X}\boldsymbol{p}_{i}$, with = $X = \{C, R_0\}$. The two sets of coordinates are then processed through an Iterative Closest Point (ICP) algorithm for estimating the underlying transformations. Depending on the system to be registered, the corresponding set of coordinates is acquired in a different way.

1) Optical camera registration: the coordinates ${}^{C}\boldsymbol{p}_{i}$ in the camera reference frame $\mathcal{F}_{C}$ are acquired manually by the operator through the NDI passive probe (see Fig. 3c), by

(a) (b) (c)

Fig. 5: Registration of the "patient" (transparent phantom on the table between the camera and the robot) with respect to the optical camera system. The user handles the optical passive probe to acquire the points of interest in the reference frame of the camera.

(a) (b) (c)

Fig. 6: Registration of the "patient" (transparent phantom on the table between the camera and the robot) with respect to the robot system. The user exploits the manual guidance functionalities of the designed system to manipulate the robot end-effector and place its tip in correspondance with the points of interest in the reference frame of the robot.

touching the fiducial markers with its tip. After the points have been correctly acquired in the camera reference frame $\mathcal{F}_C$, the ICP algorithm computes the resulting transformation ${}^{P}\boldsymbol{T}_{C}$. An example of the operator moving the robot to acquire the location of the points, along with the resulting estimated transformation applied in the simulated environment, is shown in Fig. 5. The final experimental reprojection error of the resulting estimated transformation was $\sim 4 \cdot 10^{-3}$[m].

2) Robot registration: the coordinates ${}^{R}\boldsymbol{p}_i$ in the robot base reference frame $\mathcal{F}_R$ of points on the target anatomy are measured in the robot reference frame through the Franka robot gripper. The built-in manual guidance control modality provided by the `libfranka` library is used to enable the user to move the gripper and position the tip over the fiducial markers. After the points have been acquired in the robot base reference frame $\mathcal{F}_R$, the ICP algorithm computes the resulting transformation ${}^{P}\boldsymbol{T}_{R}$ relating the surface and the robot reference frame. An example of the operator moving the robot to acquire the location of the points, along with the estimated transformation applied in the simulated environment, is shown in Fig. 6. In our experimental validation, the final reprojection error of the resulting estimated transformation was $\sim 2.07 \cdot 10^{-4}$ [m].

We finally highlight that, once ${}^{P}\boldsymbol{T}_{R}$ and ${}^{P}\boldsymbol{T}_{C}$ have been successfully estimated, it is possible to transfer geometric information from the robot to the camera frame and vice-versa, by computing the corresponding transformation: ${}^{R}\boldsymbol{T}_{C} = {}^{P}\boldsymbol{T}_{R}^{-1}\,{}^{P}\boldsymbol{T}_{C}$. Clearly, this transformation can be obtained through a camera-robot calibration procedure. The registration of camera and robot with respect to the patient is however a useful functionaly of the system allowing also manual or robot-assisted treatment delivery in an exclusive way.

B. Antenna reference pose determination

The reference pose of the radiative antenna frame $\mathcal{F}_{A,r}$ is issued by a treatment planner that, by exploiting the available medical images of the patient (e.g., CT scans), runs a simulation of the antenna radiation on the target anatomy to determine the reference pose that maximizes the coverage of target volume, within the antenna SAR region. The output is the rototranslation ${}^{P}\boldsymbol{T}_{A,r}$, expressing the reference position and orientation of the antenna in the patient frame $\mathcal{F}_P$, used as a target for the proper positioning of the antenna in the subsequent treatment delivery.

When a planning system is not available, ROBHOT also considers an alternative method to determine the reference pose of the antenna, by relying on the experience of the operator. In particular, the routine envisaged in the ROBHOT system relies on a template sheet placed over the target surface, and reporting the size of the antenna and the nominal SAR area. Then, the operator acquires a set of 6 reference points ${}^{C}\boldsymbol{p}_i$, $i = 1, \ldots, 6$ in the camera frame $\mathcal{F}_C$, through the passive probe tool and along the perimeter of the antenna drawn on the sheet. Finally, analogously the optical camera registration routine, an ICP routine is run to reconstruct the corresponding reference pose ${}^{C}\boldsymbol{T}_{A,r}$ of the antenna that best fits the set of measured points.

C. Intra-operative treatment delivery workflow

Once the antenna reference pose $\mathcal{F}_{A,r}$ has been determined (from pre-operative planning or through the manual optics-based registration routine, as detailed in Sect. III-B), the ROBHOT software loads, in the virtual environment: i) the 3D model of the patient's target anatomy characterized by

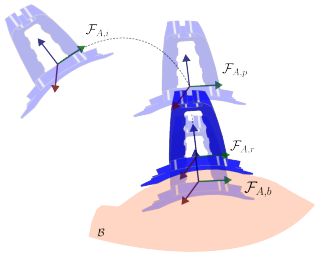

Fig. 7: Regulation of the antenna to the reference pose through a preliminary motion to the *proxy* pose $\mathcal{F}_{A,p}$ of the antenna frame.

the frame $\mathcal{F}_P$; ii) the transformation matrices ${}^{P}\boldsymbol{T}_{C}$ and ${}^{P}\boldsymbol{T}_{R}$ reporting the relative poses of the optical camera and of the robot base, respectively, resulting from the registration routines; the reference pose of the antenna $\mathcal{F}_{A,r}$ (reported as the transformation matrix ${}^{P}\boldsymbol{T}_{A,r}$ or ${}^{C}\boldsymbol{T}_{A,r}$, depending on the adopted planning routines explained in Sect. III-B).

To drive the radiative antenna, mounted at the end-effector of the robot, towards the reference pose and maintain a controlled and safe contact with the patient's body to successfully deliver the treatment, the ROBHOT system workflow considers three distinct operational modes. These modes may serve as alternative or complementary methods to complete the procedure and consist in:

1) ***Manual guidance***: the operator manipulates the radiative antenna by applying forces, such as pushing or pulling, directly to the robot manipulator arm. The robot pose is tracked and visualised in the virtual environment;

2) ***Autonomous antenna reference pose regulation***: the autonomous control regulates the antenna initial pose ${}^{R}\boldsymbol{T}_{A,i}$ to an intermediate *proxy* pose ${}^{R}\boldsymbol{T}_{A,p}$. The *proxy* pose is selected by shifting the reference ${}^{R}\boldsymbol{T}_{A,r}$ along the positive direction of the vertical axis of $\mathcal{F}_A$ (blue axis in Fig. 7), so as to initially prevent contacts with the patient's anatomy. This phase may proceed after a previous *manual guidance* mode, allowing for finer adjustments to a previous operator's positioning, or even replaces it entirely. In this latter case, autonomous control can directly take over, guiding the antenna to its reference pose from any initial robot configuration;

3) ***Autonomous interaction control***: following the *Autonomous antenna reference pose regulation* mode, this phase manages the approach of the antenna to the patient's anatomy to achieve controlled contact.

IV. Robot control

Autonomous placement of the radiative antenna in the considered clinical scenario should take into account the control of the prolonged physical contact between the antenna and the patient during the treatment. In particular, to guarantee the effectiveness of the procedure, the control must be designed so as to guarantee: i) a stable interaction with limited force magnitude; ii) a reactive behavior of the robot, to accomodate movements of the patient.

Additionally, due to possible limitations introduced by compatibility certificates and legal approvals of novel systems in the clinical environments, the criteria leading the design of the overall system should consider a minimum number of additional devices. Therefore, we did not consider any dedicated F/T sensor at the robot end-effector for the direct acquisition of interaction force measurements. We highlight, however, that the presence of torque sensors at the robot joints, along with the knowledge of the robot dynamic model, still allows to retrieve an estimation of the interaction forces through momentum-based observers [24].

An *impedance* control scheme turned out to suit the given experimental setup. The interacting environment (here, the patient body) is modeled as a mechanical system with finite stiffness, i.e., it is subject to small deformations due to external forces. In fact, as detailed below, this scheme allows to indirectly control the interaction force by regulating a Cartesian pose error, with control gains tuned in such a way to shape properly the desired interaction and achieve stiffer or softer dynamic behaviors. Moreover, as detailed below, under certain circumstances this scheme achieves indirect force regulation without relying on direct force measurements.

The design of an impedance control scheme exploits the knowledge of the robot dynamic model

$$\boldsymbol{M}(\boldsymbol{q})\ddot{\boldsymbol{q}} + \boldsymbol{C}(\boldsymbol{q},\dot{\boldsymbol{q}})\dot{\boldsymbol{q}} + \boldsymbol{g}(\boldsymbol{q}) + \boldsymbol{\tau}_f = \boldsymbol{\tau} + \boldsymbol{J}(\boldsymbol{q})^T\boldsymbol{F}_{ext}, \quad (1)$$

where $\boldsymbol{M}(\boldsymbol{q}) \in \mathbb{R}^{n\times n}$ is the inertia matrix, $\boldsymbol{C}(\boldsymbol{q},\dot{\boldsymbol{q}}) \in \mathbb{R}^{n\times n}$ is the matrix of Coriolis and centrifugal forces, $\boldsymbol{g}(\boldsymbol{q}) \in \mathbb{R}^n$ is the gravity vector and $\boldsymbol{\tau}_f \in \mathbb{R}^n$ the friction torques.

The desired behavior of the interaction between the robot and the environment ia typically modeled as a linear mass-spring-damper system:

$$\boldsymbol{M}_m\boldsymbol{\Delta}\ddot{\boldsymbol{x}} + \boldsymbol{D}_m\boldsymbol{\Delta}\dot{\boldsymbol{x}} + \boldsymbol{K}_m\boldsymbol{\Delta}\boldsymbol{x} = \boldsymbol{F}_{ext} \quad (2)$$

where $\boldsymbol{M}_m$, $\boldsymbol{D}_m$ and $\boldsymbol{K}_m$ are desired inertia, damping and stiffness matrices, respectively, while $\boldsymbol{\Delta}\boldsymbol{x} = \boldsymbol{x} - \boldsymbol{x}_d$ denotes the error of the robot end-effector pose $\boldsymbol{x}$ with respect to the desired reference $\boldsymbol{x}_d$. It can be shown that the torque control input $\boldsymbol{\tau}$ that achieves the desired interaction (2) is given by:

$$\begin{aligned}\boldsymbol{\tau} \;=\; & \boldsymbol{n}(\boldsymbol{q},\dot{\boldsymbol{q}}) + \boldsymbol{M}(\boldsymbol{q})\boldsymbol{J}^{-1}\left(\ddot{\boldsymbol{x}}_d - \dot{\boldsymbol{J}}(\boldsymbol{q})\dot{\boldsymbol{q}} + \boldsymbol{M}_m^{-1}\boldsymbol{u}_{PD}\right) \\ & + \boldsymbol{J}(\boldsymbol{q})^T\left(\boldsymbol{M}_{\boldsymbol{x}}(\boldsymbol{q})\boldsymbol{M}_m^{-1} - \boldsymbol{I}\right)\boldsymbol{F}_{ext}\end{aligned} \quad (3)$$

where $\boldsymbol{u}_{PD} = (\boldsymbol{D}_m\boldsymbol{\Delta}\dot{\boldsymbol{x}} + \boldsymbol{K}_m\boldsymbol{\Delta}\boldsymbol{x})$, $\boldsymbol{n}(\boldsymbol{q},\dot{\boldsymbol{q}}) = \boldsymbol{C}(\boldsymbol{q},\dot{\boldsymbol{q}})\dot{\boldsymbol{q}} + \boldsymbol{g}(\boldsymbol{q})$ and $\boldsymbol{M}_{\boldsymbol{x}}(\boldsymbol{q})$ is the robot Cartesian inertia matrix.

Clearly, if $\boldsymbol{M}_m = \boldsymbol{M}_{\boldsymbol{x}}(\boldsymbol{q})$, the control law (3) does not depend on the measured contact force $\boldsymbol{F}_{ext}$. However, this also alters the nature of the desired interaction model (2), that becomes nonlinear due to the presence of a configuration-dependent inertia matrix. In order to preserve the physical feasibility of the desired interaction to achieve, a Coriolis/centrifugal term should also be added to the damping term, resulting in the following nonlinear desired interaction model:

$$\boldsymbol{M}_{\boldsymbol{x}}(\boldsymbol{q})\boldsymbol{\Delta}\ddot{\boldsymbol{x}} + (\boldsymbol{D}_m + \boldsymbol{C}_{\boldsymbol{x}}(\boldsymbol{q},\dot{\boldsymbol{q}}))\,\boldsymbol{\Delta}\dot{\boldsymbol{x}} + \boldsymbol{K}_m\boldsymbol{\Delta}\boldsymbol{x} = \boldsymbol{F}_{ext} \quad (4)$$

that is achieved through the control input

$$\boldsymbol{\tau} = \boldsymbol{M}\boldsymbol{J}^{\#}\left(\ddot{\boldsymbol{x}}_d - \dot{\boldsymbol{J}}\boldsymbol{J}^{\#}\dot{\boldsymbol{x}}_d\right) + \boldsymbol{C}\boldsymbol{J}^{\#}\dot{\boldsymbol{x}}_d + \boldsymbol{g} + \boldsymbol{J}^T\boldsymbol{u}_{PD}. \quad (5)$$

The dynamic response of the closed-loop systems resulting from the control law (5) depends on the choice of the

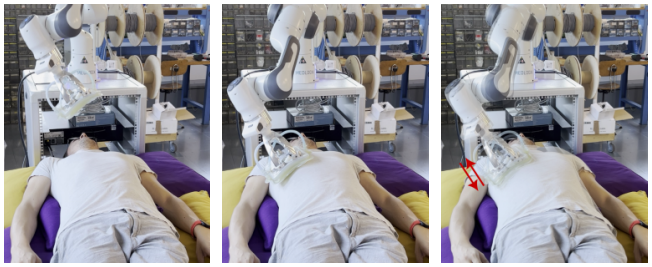

(a) (b) (c)

Fig. 8: External view of the different phases of the robot-assisted antenna positioning procedure: (a) approaching; (b) achieving contact; (c) breathing adaptation based on impedance control.

impedance gains $\boldsymbol{D}_m$ and $\boldsymbol{K}_m$. The desired impedance model shaping allows to keep limited contact forces while ensuring a desired dynamic behaviour in terms of stiffness/compliance.

In the considered scheme, the interaction force is generated since the desired reference pose of the antenna is chosen intentionally slightly *inside* the environment, so as to drive the antenna towards the body surface and produce the intended collision. The displacement of the reference pose also affects the magnitude of the interaction forces, resulting as an additional design choice in the shaping of the desired impedance model. Details about the experimental validation are provided in Section V.

V. Experimental results

This section reports on the experimental validation of interaction control in a simulated robot-assisted hyperthermia treatment delivered to a healthy human subject. First, a predefined antenna reference pose ${}^R\boldsymbol{T}_{A,r}$ in $\mathcal{F}_R$ is selected to place it in contact with the subject's chest (refer to Fig. 8). From this, the proxy pose ${}^R\boldsymbol{T}_{A,p}$ is then defined. The body reference pose ${}^R\boldsymbol{T}_{A,b}$ is finally placed a few centimeters below the reference pose along the antenna z-axis.

With reference to the operating modalities described in Sect. III, for the considered experiment, the chosen initial operating mode was the "***Autonomous antenna reference pose regulation***", with the robot autonomously driving the antenna towards the predefined reference pose (see Fig. 8a).To facilitate a smoother convergence of the antenna towards the reference pose and mitigate sharp peaks in initial torque control input, we generate a trajectory with a linear Cartesian path between the initial antenna pose ${}^R\boldsymbol{T}_{A,i}$ and the *proxy* reference pose ${}^R\boldsymbol{T}_{A,p}$, traversed according to a bang-coast-bang acceleration profile. The resulting planned trajectory will enable the antenna to accelerate with maximum acceleration a_{max}, until reaching a constant velocity v_{max}. The velocity is maintained as it approaches to the reference pose and, upon nearing the reference pose, the antenna decelerates, gradually reducing its velocity to achieve precise alignment. For the considered experiment, we set $v_{max} = 0.2[m/s]$ and $a_{max} = 0.25[m/s^2]$. To accurately track the resulting trajectory, a *stiff* dynamic behavior is imposed on the system along all the directions of the control space through the impedance control law (5), having $\boldsymbol{K}_m = \text{diag}(3\cdot10^3, 3\cdot10^3, 3\cdot10^3, 2\cdot10^2, 2\cdot10^2, 2\cdot10^2)$ and $\boldsymbol{D}_m = \text{diag}(5\cdot10, 5\cdot10, 5\cdot10, 5, 5, 5)$. The tracking performance along the planned linear Cartesian path are exhibited in the shaded blue-colored range of plots in Fig. 9-10, in the time interval $(0-6.5)$s, showing low errors both in position (p) and orientation (o).

Once the antenna *proxy* pose ${}^R\boldsymbol{T}_{A,p}$ is reached, the system enters in "***Autonomous interaction control***" mode. In this phase, the autonomous control assumes the *body* reference pose ${}^R\boldsymbol{T}_{A,b}$ as new target pose of the antenna and a linear Cartesian path is analogously interpolated, to smoothly converge and mitigate sharp control input peaks. However, differently from the previous phase, we selectively adapt the dynamic behavior of the antenna motion, so as to be *stiff* only along determined directions: to accommodate the physiological motions of the patient, such as breathing, the interaction control is designed to exhibit *compliant* behavior along the vertical axis (z) of the antenna frame ($\mathcal{F}_A$) for position regulation, and around the two planar axes (x and y) for orientation regulation. Consistently, the control strategy imposes a *stiff* behavior along the planar axes x and y for position regulation, as well as around the vertical axis z for orientation regulation. This is obtained by setting $\boldsymbol{K}_m = \text{diag}(3\cdot10^3, 3\cdot10^3, 3\cdot10^3, 2\cdot10^2, 2\cdot10^2, 2\cdot10^2)$ and $\boldsymbol{D}_m = \text{diag}(5\cdot10, 5\cdot10, 5\cdot10, 5, 5, 5)$. The resulting imposed dynamic behavior ensures adaptive response to the dynamic movements of the patient, while maintaining precise control over both position and orientation. The effectiveness of this strategy is highlighted in the shaded green and red-colored ranges of plots in Fig. 9- 10, covering the time interval $(6.5-30)$s. The vertical dashed line at $t = 7.5$s separates the approaching phase to the *body* pose ${}^R\boldsymbol{T}_{A,b}$ and the subsequent interaction control phase, resulting from the contact with the subject's chest (see also Fig. 8b). In particular, the plots highlights the different tracking performance in the stiff directions and in the compliant directions of the control space, as well as the oscillating profile resulting from the breathing of the human subject.

Finally, Fig. 11 shows the Cartesian forces and torques resulting from the interaction of the antenna with the human subject's chest, as shown also in Fig.8c. Peak values of the interaction force can be modified through the impedance model parameters, while the oscillatory behaviour can only be reduced through a feedforward action that compensates the breathing cyclic motion. To this aim, future work include a real-time tracking of the interested body area. A video clip presenting the system overview and the experiments is available at `https://youtu.be/rNxMaD-teNo`.

References

[1] N. R. Datta, E. Puric, D. Klingbiel, S. Gomez, and S. Bodis, "Hyperthermia and radiation therapy in locoregional recurrent breast cancers: A systematic review and meta-analysis," *Int. Journal of Radiation Oncology*Biology*Physics*, vol. 94, no. 5, pp. 1073–1087, 2016.

[2] P. B. Elming, B. S. Sørensen, *et al.*, "Hyperthermia: The optimal treatment to overcome radiation resistant hypoxia," *Cancers*, 2019.

[3] M. Hurwitz and P. Stauffer, "Hyperthermia, radiation and chemotherapy: The role of heat in multidisciplinary cancer care," *Seminars in Oncology*, vol. 41, no. 6, pp. 714–729, 2014.

[4] W. C. Dewey, L. E. Hopwood, S. A. Sapareto, and L. E. Gerweck, "Cellular responses to combinations of hyperthermia and radiation," *Radiology*, vol. 123, no. 2, pp. 463–474, 1977.

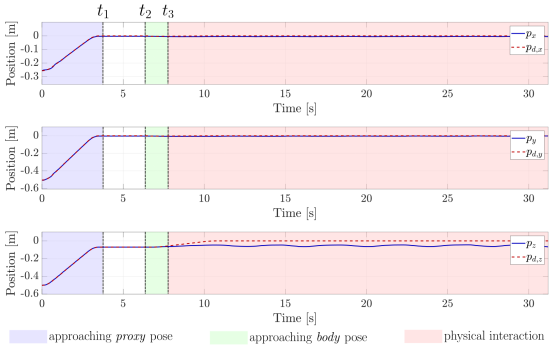

Fig. 9: Position tracking performance: autonomous regulation of the antenna to the *proxy* pose ${}^{R}\boldsymbol{T}_{A,p}$ (shaded blue interval), achieved at $t_1 = 3.5$s; autonomous regulation of the antenna to the *body* pose ${}^{R}\boldsymbol{T}_{A,b}$ (shaded green interval), started at $t_2 = 6.5$s; the physical interaction phase (shaded red interval), resulting from the contact event between the antenna and the human subject's chest, occurring at $t_3 = 7.5$s. The target pose is pourposedly set to be not reachable by the antenna, being placed "within" the body.

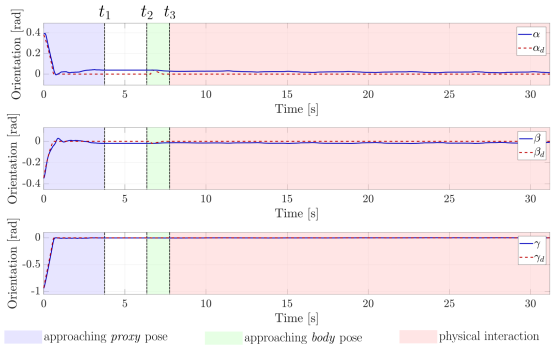

Fig. 10: Orientation tracking performance during the physical interaction between the antenna and the human subject. Time instants t_1, t_2 and t_3 and the shaded area as in Fig. 9.

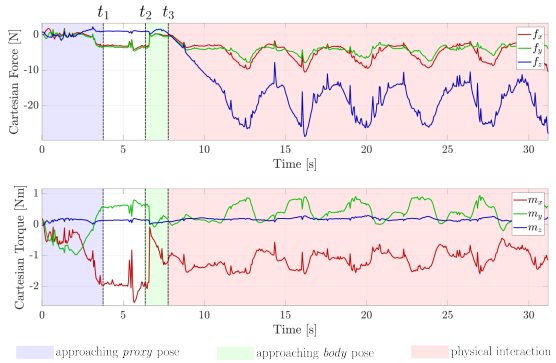

Fig. 11: Cartesian forces resulting from the physical interaction between the antenna and the human subject. Time instants t_1, t_2 and t_3 and the shaded area as in Fig. 9.

[5] B. Hildebrandt, P. Wust, O. Ahlers, A. Dieing, G. Sreenivasa, T. Kerner, R. Felix, and H. Riess, "The cellular and molecular basis of hyperthermia," *Critical Reviews in Oncology/Hematology*, vol. 43, no. 1, pp. 33–56, 2002.

[6] A. Oei, L. Vriend, J. Crezee, *et al.*, "Effects of hyperthermia on dna repair pathways: one treatment to inhibit them all," *Radiat Oncol*, vol. 10, no. 165, 2015.

[7] C. van Leeuwen, A. Oei, K. Chin, H. Crezee, A. Bel, A. Westermann, M. Buist, N. Franken, L. Stalpers, and H. Kok, "A short time interval between radiotherapy and hyperthermia reduces in-field recurrence and mortality in women with advanced cervical cancer," *Radiation Oncology*, vol. 12, 04 2017.

[8] H. Crezee, H. P. Kok, A. L. Oei, N. A. P. Franken, and L. J. A. Stalpers, "The impact of the time interval between radiation and hyperthermia on clinical outcome in patients with locally advanced cervical cancer," *Frontiers in Oncology*, vol. 9, 2019.

[9] A. Bakker, J. van der Zee, G. van Tienhoven, H. P. Kok, C. R. N. Rasch, and H. Crezee, "Temperature and thermal dose during radiotherapy and hyperthermia for recurrent breast cancer are related to clinical outcome and thermal toxicity: a systematic review," *International Journal of Hyperthermia*, vol. 36, no. 1, pp. 1023–1038, 2019.

[10] M. D. Greef, H. P. Kok, A. Bel, and J. Crezee, "3d versus 2d steering in patient anatomies: A comparison using hyperthermia treatment planning," *Int. J. of Hyperthermia*, vol. 27, no. 1, pp. 74–85, 2011.

[11] B. S. C. R. e. a. Bruggmoser, G., "Guideline for the clinical application, documentation and analysis of clinical studies for regional deep hyperthermia," *Strahlenther Onkol*, vol. 188, no. 2, p. 198–211, 2012.

[12] J. W. S. III, N. R. Datta, and Z. Vujaskovic, "Hyperthermia and radiotherapy in bladder cancer," *International Journal of Hyperthermia*, vol. 32, no. 4, pp. 398–406, 2016.

[13] T. Ohguri, Y. Harima, H. Imada, H. Sakurai, T. Ohno, Y. Hiraki, K. Tuji, M. Tanaka, and H. Terashima, "Relationships between thermal dose parameters and the efficacy of definitive chemoradiotherapy plus regional hyperthermia in the treatment of locally advanced cervical cancer: data from a multicentre randomised clinical trial," *International Journal of Hyperthermia*, vol. 34, no. 4, pp. 461–468, 2018.

[14] W. P. S. P. e. a. Kok, H., "Current state of the art of regional hyperthermia treatment planning: a review," *Radiat Oncol*, vol. 10, no. 196, 2015.

[15] A. Mariani, L. Morchi, A. Diodato, S. Tognarelli, and A. Menciassi, "High-intensity focused ultrasound surgery based on kuka robot: A computer-assisted platform for noninvasive surgical treatments on static and moving organs," *IEEE Robotics Automation Magazine*, vol. 30, no. 3, pp. 79–93, 2023.

[16] P. Besl and N. D. McKay, "A method for registration of 3-d shapes," *IEEE Transactions on Pattern Analysis and Machine Intelligence*, vol. 14, no. 2, pp. 239–256, 1992.

[17] B. Siciliano and O. Khatib, *Springer Handbook of Robotics*, 2016.

[18] T. Haidegger, B. Benyó, L. Kovács, and Z. Benyó, "Force sensing and force control for surgical robots," *IFAC Proceedings Volumes*, vol. 42, no. 12, pp. 401–406, 2009.

[19] C. Sousa, R. Cortesao, and P. Queiros, "Compliant comanipulation control for medical robotics," in *2009 2nd Conference on Human System Interactions*, 2009, pp. 265–271.

[20] P. Chatelain, A. Krupa, and N. Navab, "Confidence-driven control of an ultrasound probe," *IEEE Transactions on Robotics*, vol. 33, no. 6, pp. 1410–1424, 2017.

[21] L. Cheng and M. Tavakoli, "Ultrasound image guidance and robot impedance control for beating-heart surgery," *Control Engineering Practice*, vol. 81, pp. 9–17, 2018.

[22] M. Dyck, A. Weld, J. Klodmann, *et al.*, "Toward safe and collaborative robotic ultrasound tissue scanning in neurosurgery," *IEEE Transactions on Medical Robotics and Bionics*, vol. 6, no. 1, pp. 64–67, 2024.

[23] M. Ferro, C. Gaz, M. Anzidei, and M. Vendittelli, "Online needle-tissue interaction model identification for force feedback enhancement in robot-assisted interventional procedures," *IEEE Transactions on Medical Robotics and Bionics*, vol. 3, no. 4, pp. 936–947, 2021.

[24] S. Haddadin, A. De Luca, and A. Albu-Schäffer, "Robot collisions: A survey on detection, isolation, and identification," *IEEE Transactions on Robotics*, vol. 33, no. 6, pp. 1292–1312, 2017.

[25] A. Cristofaro, G. Cappellini, E. Staffetti, G. Trappolini, and M. Vendittelli, "Adaptive estimation of the pennes' bio-heat equation - i: Observer design," in *2023 62nd IEEE Conf. on Decision and Control (CDC)*, 2023, pp. 1931–1936.

[26] G. Cappellini, G. Trappolini, E. Staffetti, A. Cristofaro, and M. Vendittelli, "Adaptive estimation of the pennes' bio-heat equation - ii: A nn-based implementation for real-time applications," in *2023 62nd IEEE Conf on Decision and Control (CDC)*, 2023, pp. 5364–5369.

VI. Conclusions

We have presented a new system for robot-assisted superficial hyperthermia allowing to achieve the unprecedent accuracy in treatment delivery while guaranteeing safety of the patient. In future work we will include tracking of human motion to reduce the oscillation in the interaction force and a non-invasive temperature estimation at the target using the method developed in [25] and [26].